Solid State Sciences 66 (2017) 44–49

Contents lists available at ScienceDirect

Solid State Sciences

journal homepage: www.elsevier.com/locate/ssscie

Well-dispersed sulfur anchored on interconnected polypyrrole nanofiber network as high performance cathode for lithium-sulfur batteries

Fuxing Yin [a, b], Xinyi Liu [a, b, c], Yongguang Zhang [a, b, *], Yan Zhao [a, b], Almagul Menbayeva [d], Zhumabay Bakenov [d], Xin Wang [e, **]

[a] Research Institute for Energy Equipment Materials, Hebei University of Technology, Tianjin 300130, China
[b] Tianjin Key Laboratory of Materials Laminating Fabrication and Interface Control Technology, Hebei University of Technology, Tianjin 300130, China
[c] School of Material Science & Engineering, Hebei University of Technology, Tianjin 300130 China
[d] Institute of Batteries LLC, National Laboratory Astana, Nazarbayev University, 53 Kabanbay Batyr Avenue, Astana 010000, Kazakhstan
[e] Institute of Electronic Paper Displays, South China Academy of Advanced Optoelectronics, South China Normal University, Guangzhou, Guangdong Province, China

ARTICLE INFO

Article history:
Received 26 May 2016
Received in revised form
6 December 2016
Accepted 23 February 2017
Available online 3 March 2017

Keywords:
Lithium/sulfur battery
Nanostructured sulfur cathode
PPy nanowire network
S/PPy composite

ABSTRACT

Preparation of novel sulfur/polypyrrole (S/PPy) composite consisting well-dispersed sulfur particles anchored on interconnected PPy nanowire network was demonstrated. In such hybrid structure, the as-prepared PPy clearly displays a three-dimensionally cross-linked and hierarchical porous structure, which was utilized in the composite cathode as a conductive network trapping soluble polysulfide intermediates and enhancing the overall electrochemical performance of the system. Benefiting from this unique structure, the S/PPy composite demonstrated excellent cycling stability, resulting in a discharge capacity of 931 mAh g^{-1} at the second cycle and retained about 54% of this value over 100 cycles at 0.1 C. Furthermore, the S/PPy composite cathode exhibits a good rate capability with a discharge capacity of 584 mAh g^{-1} at 1 C.

1. Introduction

Secondary lithium-ion batteries (LIBs) are leading the market for power sources for portable electronics such as cellular phones, notebook computers, and camcorders. However, the use of this battery technology in electric and hybrid electric vehicles (EV and HEV) and large-scale stationary energy storage systems still needs further enhancement in terms of cathode capacity and rate performance [1,2].

Elemental sulfur (S) is a promising cathode material for the next generation high-energy rechargeable lithium batteries due to its low cost, abundance, environmental friendliness, and high theoretical capacity of 1672 mAh g^{-1} and theoretical specific energy of 2600 Wh kg^{-1} [3]. However, despite these promising metrics, lithium/sulfur (Li/S) batteries suffer from a low level of cathode material utilization and poor cycle life, which is essentially due to insulating nature of S and solubility of reductive polysulfides in liquid organic electrolyte [4,5]. Much effort has been dedicated to overcome the low conductivity issues of S cathode, including the preparation of various types of conductive sulfur/carbon [6–8] and sulfur/conductive polymer composites [9–11]. Among these, the mixtures of PPy with sulfur have been intensively scrutinized, due to the high absorption ability of PPy, which can prevent dissolution of polysulfides into the electrolyte [9].

Some previous studies have confirmed that interconnected conductive polymer (such as polyaniline and polypyrrole) network can work as a good support for inorganic oxide as a LIB anode, effectively enhancing the structural stability of electrode materials and avoiding the dissolution and aggregation of electrode nanomaterials [12–15]. Taking into account, such effects, the interconnected conductive polymers could also be utilized as conductive network and structural skeleton for sulfur cathode to improve its electrochemical performance. Herein, we report on synthesis of a composite, where sulfur nanoparticles are anchored

* Corresponding author. Research Institute for Energy Equipment Materials, Hebei University of Technology, Tianjin 300130, China.
** Corresponding author.
E-mail addresses: yongguangzhang@hebut.edu.cn (Y. Zhang), wangxin@scnu.edu.cn (X. Wang).

http://dx.doi.org/10.1016/j.solidstatesciences.2017.02.009

on interconnected polypyrrole nanowire network, as cathode for Li/S batteries, and studies of its composition, structure and electrochemical performance.

2. Experimental

2.1. Material synthesis

Polypyrrole was prepared by the method described by Zhang et al. [16], with some modifications of the process. 0.127 g cetyltrimethylammonium bromide (CTAB) (Tianjin Guangfu, ≥ 99% purity), was dissolved in 100 mL deionized water. Afterwards, 0.346 mL pyrrole (Py) monomer (Tianjin Fuchen, ≥ 99% purity) was added into the CTAB solution with stirring for 0.5 h. Further, 1.141 g ammonium persulfate (APS) (Tianjin Kewei, ≥ 98% purity) was dissolved in 50 mL deionized water as an oxidizing agent, and added into the CTAB/Py mixture to initiate polymerization. The resultant solution was stirred for 24 h. All synthesis procedures were carried out within a temperature range of 0–5 °C. The precipitate of PPy, formed upon the reaction, was separated via filtration and thoroughly washed by deionized water and ethanol, and then dried overnight at 60 °C. A black powder of polypyrrole was finally obtained.

The S/PPy composites were prepared via a simple ball-milling followed by a low-temperature heat treatment. Typically, 0.2 g of as prepared PPy was mixed with 4 g of nano-sulfur aqueous suspension (US Nanomaterials, 10 wt%) by ball-milling at 600 rpm for 3 h, and then dried at 60 °C overnight to remove the solvent. The resulting mixture was heated at 150 °C for 3 h in argon gas to obtain a desired S/PPy composite.

2.2. Material characterization

The surface morphology information of the samples was obtained from field emission scanning electron microscopy (FE-SEM, S-4800, Hitachi Ltd.). The interior structure of the samples was observed using transmission electron microscopy (TEM, JEM-2100F, JEOL). Crystal structural characterizations were determined by X-ray diffractometer (XRD, Smart Lab, Rigaku Corporation). The S content in the S/PPy composite was determined using chemical analysis (CHNS, Vario Micro Cube, Elementar). The chemical transformation of the samples was carried out with Fourier transform infrared spectroscopy (FTIR, TENSOR 27, BRUKER). The specific surface area was examined by the Brunaner-Emmet-Teller (BET) and Barret-Joyner-Halenda (BJH) methods at 77 K (Autosorb iQ, Quantachrome Corporation). X-Ray photoelectron spectroscopy (XPS) data were obtained with a PHI Quantera electron spectrometer using AlKα radiation. Thermogravimetric analysis (TGA, SDT Q-600, TA Instruments-Waters LLC) was conducted under Ar atmosphere with a heating rate of 10 °C min^{-1}.

2.3. Electrochemical measurements

The electrochemical performance of the S/PPy composite was investigated using coin-type cells (CR2025). The cell was composed of lithium metal anode and S/PPy composite cathode separated by a microporous polypropylene separator soaked in 1 M lithium trifluoromethanesulfonate ($LiCF_3SO_4$) in dimethoxy ethane (DME) and 1,3-dioxolane (DOL) (1:1 v/v) electrolyte. The composite cathode was prepared by mixing 80 wt% S/PPy composite, 10 wt% polyvinylidene fluoride (PVDF) (Kynar, HSV900) as a binder and 10 wt% acetylene black (MTI, 99.5% purity) conducting agent in 1-methyl-2-pyrrolidinone (NMP, Sigma-Aldrich, ≥99.5% purity). The resultant slurry was uniformly spread onto aluminum foil using a doctor blade, and dried at 50 °C for 12 h. The resulting cathode sheet was used to prepare the cathodes by punching circular disks with 1 cm in diameter. The sulfur loading in each electrode was about 4 mg cm^{-2}. The coin cells were assembled in an Ar (99.9995%) filled glove box (MBraun) and tested galvanostatically on a multichannel battery tester (BTS-5V5mA, Neware, and BT-2000, Arbin Inc.) between 1.5 and 3 V *vs.* Li^+/Li at different current densities. Cyclic voltammetry (CV) measurements were performed with a potentiostat (VMP3, Biologic) between 1.5 and 3 V *vs.* Li^+/Li at a scanning rate of 0.1 mV s^{-1}. The chemical analysis of the composite has confirmed a high sulfur content of 60 wt%. Applied currents and specific capacities were calculated on the basis of the weight of S in each cathode.

3. Results and discussion

The XRD patterns of sulfur, as-prepared PPy and S/PPy composite samples are shown in Fig. 1a. One can see that as-prepared PPy displays a broad and low intensity peak around 22°, which indicates its amorphous character due to the pyrrole intermolecular spacing [17,18]. The XRD patterns of sulfur used in the work exhibits the characteristic *Fddd* orthorhombic crystal structure peaks of elemental sulfur. However, the XRD patterns of S/PPy

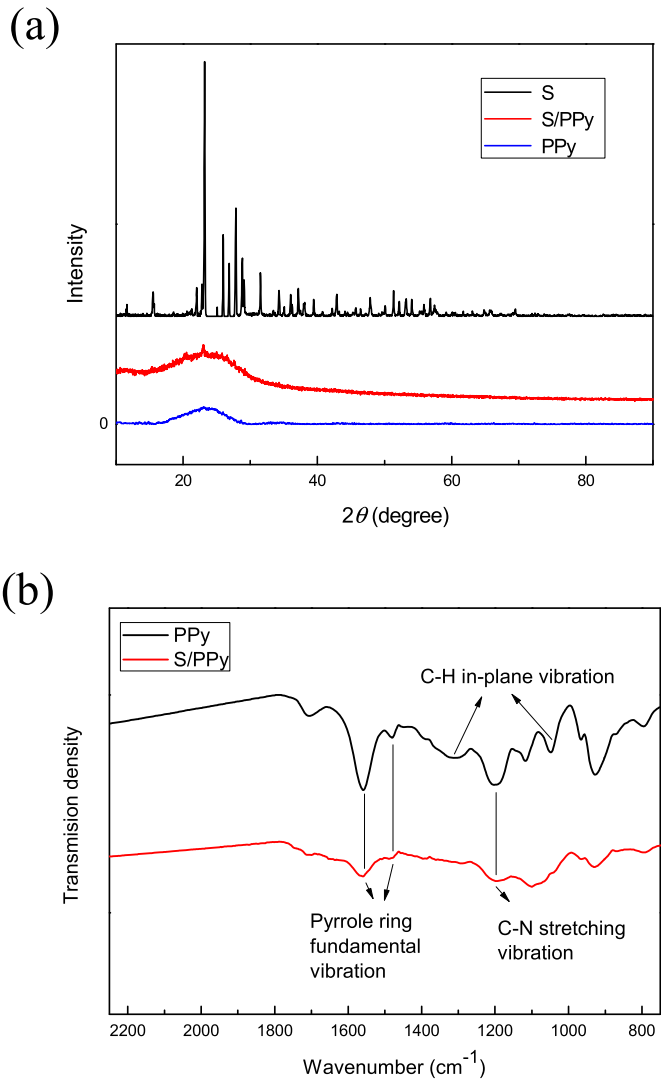

Fig. 1. (a) XRD patterns of S, PPy and S/PPy composite; (b) FTIR spectra of PPy and S/PPy composite.

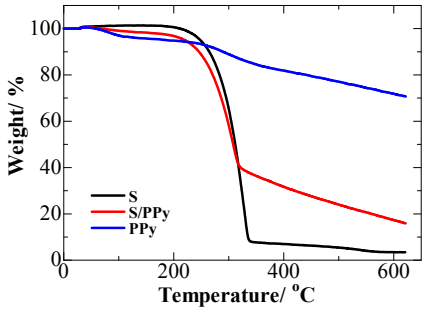

Fig. 2. TGA curves of S, PPy and S/PPy composite at a heating rate of 10 °C min^{-1}.

composite exhibit the features similar to that of PPy, a wide and low intensity peak around 22°. This likely results from the nanoscopic character of sulfur particles well-dispersed in a porous structure [18–20]. The molecular structure of as-prepared PPy and S/PPy composite were studied by the FTIR spectrum analysis as shown in Fig. 1b. It can be seen that both materials spectra are similar, which indicates that no chemical reaction between sulfur and PPy occurred during the composite preparation process. In both as prepared PPy and S/PPy composite, the characteristic peaks at 1545 cm^{-1} and 1458 cm^{-1} can be assigned to the pyrrole ring fundamental vibrations and the broad peaks at 1291 cm^{-1} and 1043 cm^{-1} represent the = C-H in-plane vibrations and those at 1175 cm^{-1} were related to the C-N stretching vibration. This matches well with the literature data [21–24]. These results confirm successful preparation of PPy structure via *in situ* chemical polymerization method.

Fig. 2 presents of the TGA curves of S, PPy and the S/PPy composite. One can see that the weight loss curve of the sample can be divided into two regions. At the temperature range of 100–200 °C the sample loses about 5% of its weight, which is due to the evaporation of water. For both sulfur and S/PPy composite, there is a rapid weight loss when the temperature was further increases from 200 to 300 °C: while the S sample was completely evaporated, the S/PPy rapid losses about 60% of its weight. This tendency comparison allowed us to attribute the weight loss in the composite to the sublimation of sulfur from the highly porous structure of the composite. It can be seen that when the temperature was further increased up to 600 °C, there is no significant change in the sample weight. Therefore, the amount of sulfur in the composite could be estimated as ~60 wt%, which perfectly matches with the results obtained by the CHNS chemical analysis.

The results of investigation of specific surface area and pore size distribution of both as-prepared PPy and S/PPy composite are shown in Fig. 3. The N_2 adsorption/desorption isotherm of PPy shows a large BET specific surface area of 93.081 $m^2\ g^{-1}$ with the pore volume of 0.573 $cm^3\ g^{-1}$ and the average pore size of 1.194 nm.

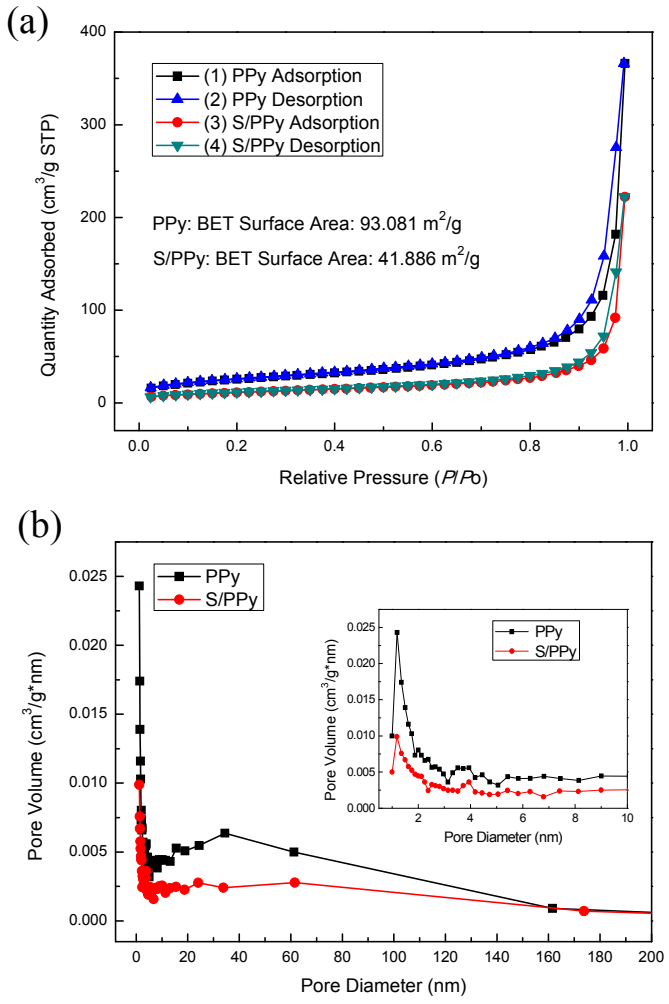

Fig. 3. (a) N_2 adsorption-desorption isotherms; (b) Pore size distribution of PPy and S/PPy composite. Inset: magnification of pore size distribution between 1 and 10.0 nm.

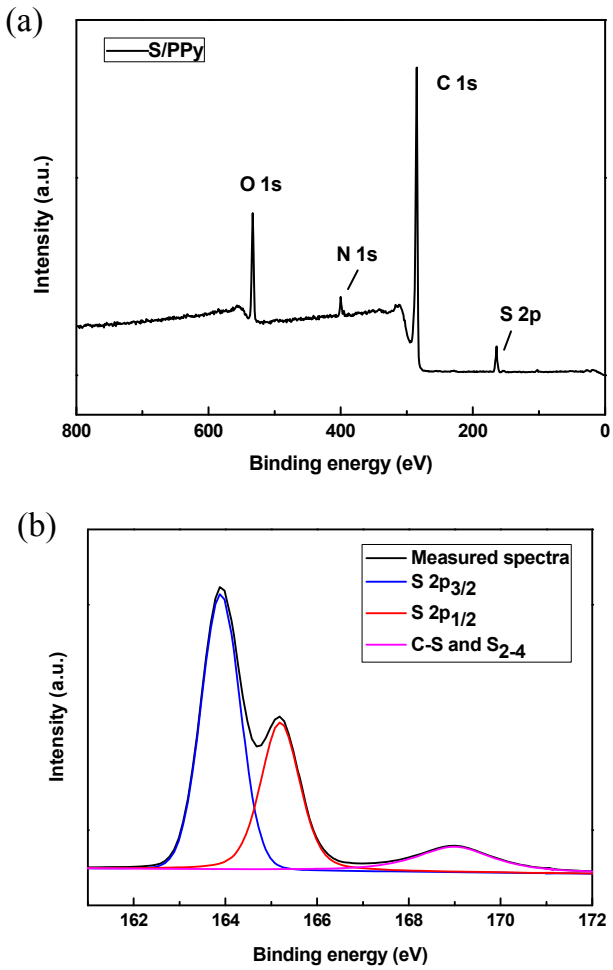

Fig. 4. (a) XPS survey spectra of S/PPy and (b) high-resolution XPS spectra of S 2p.

This indicates that large micropores and mesopores are embedded in the surface of PPy network. After compositing with sulfur, the specific surface area of sample decreases to 41.886 $m^2\ g^{-1}$ and the pore volume decreases to 0.349 $cm^3\ g^{-1}$, which could be due to deposition of a large amount of sulfur into the pores and surface of the PPy network.

To further confirm the chemical composition and surface properties of S/PPy composites, the XPS measurements of the samples were performed. The survey spectra in Fig. 4a prove that four peaks at 164, 290, 401 and 530 eV could be attributed to S2p, C1s, N1s and O1s, respectively. As shown in Fig. 4b, XPS results display the S2p spectra for the S/PPy composites. The S2p peaks can be divided into two components including the S2p3/2 (163.7 eV) and S2p1/2 (165.0 eV) peaks, and another weak broad peak located between 167.5 eV and 170.5 eV, which can be attributed to the interaction between sulfur and PPy.

The surface morphology and structures of as-prepared PPy were investigated by SEM and TEM, as presented in Fig. 5a and b. The PPy clearly displays a three-dimensionally cross-linked and hierarchical porous structure, which consists of fine nanowires with a high degree of interlocking [15]. Inset in Fig. 5a presents the PPy nanowire diameter distribution obtained from the SEM data [9]. PPy nanowires have uniform diameter distribution with an average diameter of 58.3 nm. Fig. 5c reveals that the average diameter of nanowires increases after compositing with sulfur, which is in good agreement with the TEM results shown in Fig. 5d. We postulate that the nanosized sulfur is melted and absorbed by the porous surface of PPy nanowires. The elemental mapping (Fig. 5e-5g) confirms homogeneous distribution of sulfur and PPy in the S/PPy composite. This fact along with a highly porous structure of the composite could positively affect the overall electrochemical performance of the composite cathode [25], because this porous network structure of S/PPy with homogeneous distribution of sulfur could also provide a large contact interface between electrode and electrolyte and afford "buffering" space to accommodate the volume changes of sulfur upon cycling [26,27].

Fig. 6 shows the CV curves of S/PPy cathode between 1.5 V and 3 V *vs.* Li^+/Li for initial two cycles at a scan rate of 0.1 mV s^{-1}. The

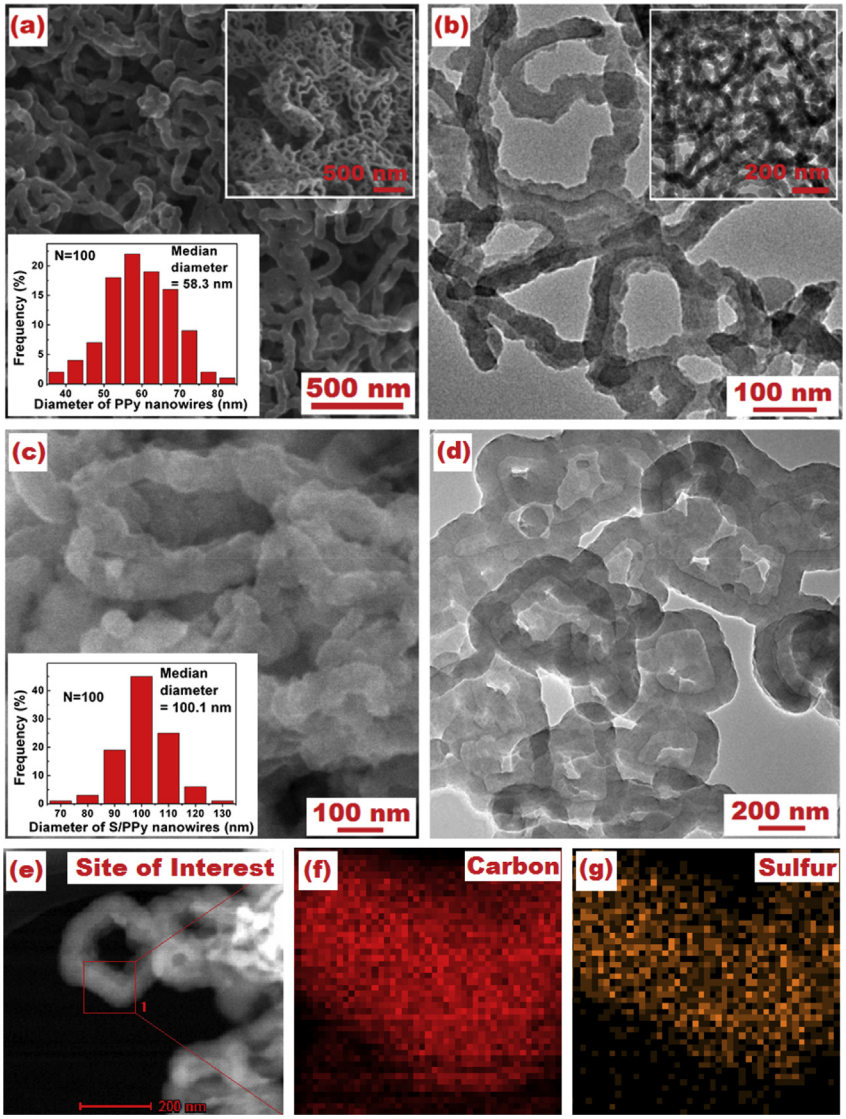

Fig. 5. (a) SEM images of PPy at different magnifications, inset: diameter distribution of the PPy nanowires; (b) TEM images of PPy at different magnifications; (c) SEM image of S/PPy composite, inset: diameter distribution of the S/PPy composite; (d) TEM image of S/PPy composite and (e-g) EDS mapping showing the distribution of sulfur (S) and carbon (C) in the S/PPy composite.

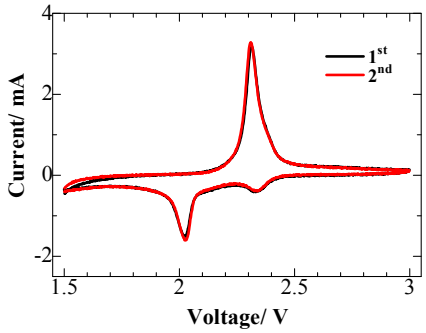

Fig. 6. CV curves of S/PPy composite (a potential sweep rate is 0.1 mV s^{-1}).

sharp redox peaks with stable overlapping features confirm high reversibility and an excellent stability of the composite electrode upon operation in lithium battery [28]. In the cathodic (reduction) sweep, the peaks at 2.4 and 2.0 V can be observed, which are assigned to the reduction of element sulfur (S_8) to soluble lithium polysulfides (Li_2S_n, $4 \leq n \leq 8$) and further conversion of these lithium polysulfides into insoluble Li_2S_2 and Li_2S, respectively [29]. The only one anodic peak at 2.4 V corresponds to the reversible transformation of Li_2S_2 and Li_2S to Li_2S_8 [30].

Fig. 7 depicts the typical initial discharge/charge voltage profiles of the S/PPy composite at 0.1 C rate (1 C = 1672 mAh g^{-1}). The discharge curves exhibited a typical two-plateau behavior of a sulfur cathode, corresponding to the formation of higher-order lithium polysulfides (Li_2S_n, $n \geq 4$) at 2.5 V and further electrochemical transition of these polysuflides to lithium sulfides (Li_2S) at 2.0 V. Moreover, the second plateau is very flat, suggesting a uniform deposition of Li_2S [31]. The S/PPy composite delivers a high initial discharge capacity of about 1051 mAh g^{-1} at 0.1 C, and it still maintains a high reversible discharge capacity of about 883 mAh g^{-1} at the third cycle, exhibiting a high electrochemical reversibility. The cycling behavior of the S/PPy composite is presented in Fig. 8. The discharge capacity of S/PPy composite was stabilized after two cycles at 931 mAh g^{-1} and a discharge capacity of 503 mAh g^{-1} was retained after 100 cycles, representing a good cycle stability. This indicates that PPy network in the composite plays a significant role in suppressing the shuttle effect via absorption of the polysulfides formed in the electrochemical reaction. Fig. 9 presents the rate performance of S/PPy composite. The discharge capacities of 900, 795, 687, 584 mAh g^{-1} were delivered at current densities of 0.1, 0.2, 0.5 and 1 C, respectively. Moreover, the capacity of the composite could basically be restored to its original value when the current density is switched back to 0.1 C. The perfect rate performance of the composite cathode was ascribed to the presence of highly effective electron pathways formed by the interconnected PPy.

The electrochemical properties of the S/PPy composite cathode were further investigated using galvanostatic charge-discharge cycling at 0.5 and 1.0 C current densities. Fig. 10 presents the results of cyclic performance of the composite cathode at these conditions. It can be seen that the initial capacities of 958 mAh g^{-1} and 826 mAh g^{-1} were obtained at 0.5 C and 1 C, respectively. The discharge capacity of the cathode remained 547 mAh g^{-1} and 428 mAh g^{-1} after 50 cycles at these cycling rates, and the S/PPy composite shows a low capacity decay rate.

4. Conclusions

A novel S/PPy composite consisting well-dispersed sulfur anchored on interconnected PPy nanowire network was obtained via a simple ball-milling followed by a low-temperature heat treatment. In such a hybrid structure, PPy possesses a three-dimensionally cross-linked and hierarchical porous structure, which plays an important role in both providing adequate lithium ion transport path and retarding diffusion of polysulfides out of the

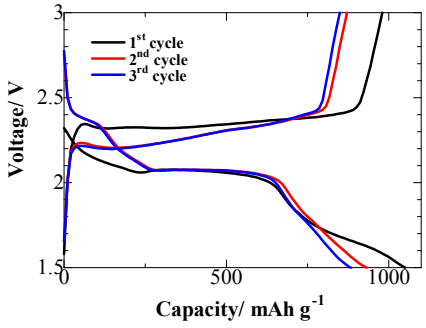

Fig. 7. Discharge/charge profiles of the S/PPy composite cathode at 0.1 C rate.

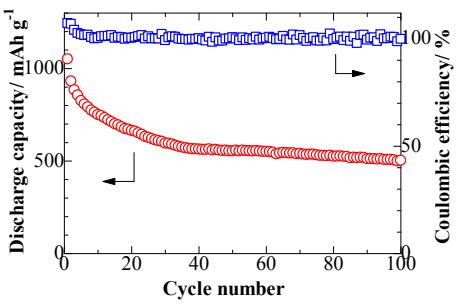

Fig. 8. Cyclability of the S/PPy composite cathode at 0.1 C rate.

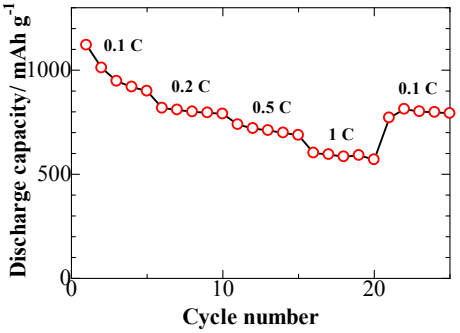

Fig. 9. Rate capability of the S/PPy composite cathode.

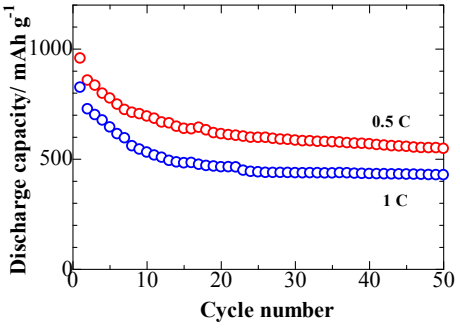

Fig. 10. Cyclability of S/PPy composite cathode at high C-rates of 0.5 C and 1 C.

cathode. Consequently, the S/PPy composite exhibits good cycling and rate capability as a cathode for rechargeable lithium/sulfur batteries.

Acknowledgements

This work was supported by the National Natural Science Foundation of China [grant number 21406052]; the Program for the Outstanding Young Talents of Hebei Province [grant number BJ2014010]; the Science Research Foundation for Selected Overseas Chinese Scholars, Ministry of Human Resources and Social Security of China [grant number CG2015003002]; the Pearl River S&T Nova Program of Guangzhou [grant number 201506040045] and the Ministry of Education and Science of Kazakhstan [grant number 4649/GF and 5156GF, and the targeted program N⁰0115PK03029].

References

[1] B. Kang, G. Ceder, Battery materials for ultrafast charging and discharging, Nature 458 (2009) 190–193.
[2] M. Armand, J.M. Tarascon, Building better batteries, Development in lithium/sulfur secondary batteries, Nature 451 (2008) 652–657.
[3] Y. Zhang, Y. Zhao, K.E.K. Sun, P. Chen, Development in lithium/sulfur secondary batteries, Open Mater Sci. J. 5 (2011) 215–221.
[4] R.J. Chen, T. Zhao, F. Wu, From a historic review to horizons beyond: lithium-sulfur batteries run on the wheels, Chem. Commun. 51 (2015) 18–33.
[5] X. Fang, H.S. Peng, A revolution in electrodes: recent progress in rechargeable lithium-sulfur batteries, Small 11 (2015) 1488–1511.
[6] Y. Zhao, Y. Zhang, Z. Bakenov, P. Chen, Electrochemical performance of lithium gel polymer battery with nanostructured sulfur/carbon composite cathode, Solid State Ionics 234 (2013) 40–45.
[7] Y. Zhang, Y. Zhao, A. Konarov, Z. Li, P. Chen, Effect of mesoporous carbon microtube prepared by carbonizing the poplar catkin on sulfur cathode performance in Li/S batteries, J. Alloys Compd. 619 (2015) 298–302.
[8] Z. Li, Y. Huang, L. Yuan, Z. Hao, Y. Huang, Status and prospects in sulfur-carbon composites as cathode materials for rechargeable lithium-sulfur batteries, Carbon 92 (2015) 41–63.
[9] Y. Zhang, Z. Bakenov, Y. Zhao, A. Konarov, T.N.L. Doan, M. Malik, One-step synthesis of branched sulfur/polypyrrole nanocomposite cathode for lithium rechargeable batteries, J. Power Sources 208 (2012) 1–8.
[10] K. Jeddi, Y. Zhao, Y. Zhang, A. Konarov, P. Chen, Fabrication and characterization of an effective polymer nanocomposite electrolyte membrane for high performance lithium/sulfur batteries, J. Electrochem Soc. 160 (2013) 1052–1060.
[11] N. Nakamura, T. Yokoshima, H. Nara, T. Momma, T. Osaka, Suppression of polysulfide dissolution by polypyrrole modification of sulfur-based cathodes in lithium secondary batteries, J. Power Sources 274 (2015) 1263–1266.
[12] Y. Zhao, J. Li, N. Wang, C. Wu, G. Dong, L. Guan, Fully reversibleconversion between SnO2 and Sn in SWNTs@SnO2@PPy coaxialnanocable as high performance anode material for lithium ion batteries, J. Phys. Chem. C 116 (2012) 18612–18617.
[13] J.F. Zhao, S.C. Zhang, W.B. Liu, Z.J. Du, H. Fang, Fe_3O_4/PPy composite nanospheres as anode for lithium-ion batteries with superior cycling performance, Electrochim. Acta 121 (2014) 428–433.
[14] Y. Mao, Q. Kong, B. Guo, L. Shen, Z. Wang L, Polypyrrole-NiO composite as high-performance lithium storage material, Electrochim. Acta 105 (2013) 162–169.
[15] X.M. Yang, J. Chen, Q.Y. Chen, X.B. Ji, Antimony nanoparticles anchored on interconnected carbon nanofibers networks as advanced anode material for sodium-ion batteries, J. power sources 284 (2015) 227–235.
[16] X.T. Zhang, J. Zhang, W.H. Song, Z.F. Liu, Controllable synthesis of conducting polypyrrole nanostructures, J. Phys. Chem. B 110 (2006) 1158–1165.
[17] T.K. Vishnuvardhan, V.R. Kulkarni, C. Basavaraja, S.C. Raghavendra, Synthesis, characterization and ac conductivity of polypyrrole/Y_2O_3 composites, Mater. Sci. 29 (2006) 77–83.
[18] C. Pirlot, I. Willems, A. Fonseca, J.B. Nagy, J. Delhalle, Preparation and characterization of carbon nanotube/polyacrylonitrile composites, Adv. Eng. Mater 4 (2002) 109–114.
[19] M. Endo, K. Takeuchi, T. Hiroka, T. Furuta, T. Kasai, X. Sun, C.H. Kiang, M.S. Dresselhaus, Stacking nature of graphene layers in carbon nanotubes and nanofibres, J. Phys. Chem. Solids 58 (1997) 1707–1712.
[20] Y. Zhang, Y. Zhao, Z. Bakenov, Synthesis of hierarchical porous sulfur/polypyrrole/multiwalled carbon nanotube composite cathode for lithium batteries, Electrochim. Acta 143 (2014) 49–55.
[21] X. Liang, Y. Liu, Z. Wen, L. Huang, X. Wang, H. Zhang, A nano-structured and highly ordered polypyrrole-sulfur cathode for lithium-sulfur batteries, J. Power Sources 196 (2011) 6951–6955.
[22] M.M. Sun, S.C. Zhang, T. Jiang, L. Zhang, J.H. Yu, Nano-wire networks of sulfur-polypyrrole composite cathode materials for rechargeable lithium batteries, Electrochem. Commun. 10 (2008) 1819–1822.
[23] J.T. Lei, W.B. Liang, C.R. Martin, Infrared investigations of pristine, doped and partially doped polypyrrole, Synth. Met. 48 (1992) 301–312.
[24] K. Cheah, M. Forsyth, V.T. Truong, Ordering and stability in conducting polypyrrole, Synth. Met. 94 (1998) 215–219.
[25] Y. Zhang, Y. Zhao, Z. Bakenov, A simple approach to synthesize nanosized sulfur/graphene oxide materials for high-performance lithium/sulfur batteries, Ionics 20 (2014) 1047–1050.
[26] Y.G. Guo, J.S. Hu, L.J. Wan, Nanostructured materials for electrochemical energy conversion and storage devices, Adv. Mater 20 (2008) 2878–2887.
[27] X.L. Wu, L.Y. Jiang, F.F. Cao, Y.G. Guo, L.J. Wan, $LiFePO_4$ nanoparticles embedded in a nanoporous carbon matrix: superior cathode material for electrochemical energy-storage devices, Adv. Mater 21 (2009) 2710–2714.
[28] B. Ding, C.Z. Yuan, L.F. Shen, G.Y. Xu, P. Nie, Q.X. Lai, X.G. Zhang, Chemically tailoring the nanostructure of graphene nanosheets to confine sulfur for high-performance lithium-sulfur batteries, J. Mater.Chem. A 1 (2013) 1096–1101.
[29] R.D. Rauh, K.M. Abraham, G.F. Pearson, J.K. Surprenant, S.B. Brummer, A lithium/dissolved sulfur battery with an organic electrolyte, J. Electrochem. Soc. 126 (1979) 523–527.
[30] C.X. Zu, A. Manthiram, Hydroxylated graphene–sulfur nanocomposites for high-rate lithium–sulfur batteries, Adv. Energy Mater 3 (2013) 1008–1012.
[31] T.Q. Lin, Y.F. Tang, Y.M. Wang, H. Bi, Z.Q. Liu, Scotch-tape-like exfoliation of graphite assisted with elemental sulfur and graphene-sulfur composites for high-performance lithium-sulfur batteries, Energy Env. Sci. 6 (2013) 1283–1290.